ELSEVIER

Physica B 323 (2002) 115–121

PHYSICA B

www.elsevier.com/locate/physb

Experimental probes of the molecular hydrogen–carbon nanotube interaction

Bhabendra K. Pradhan, Gamini U. Sumanasekera, Kofi W. Adu, Hugo E. Romero, Keith A. Williams[1], Peter C. Eklund*

Department of Physics, The Pennsylvania State University, 104 Davey Laboratory, 16802-6300 University Park, PA, USA

Abstract

Electrical transport (resistance R and thermoelectric power S), Raman scattering, and hydrogen adsorption are used to study the interaction of hydrogen molecules with ropes of single-walled carbon nanotubes. The data are consistent with H_2 physisorption under the experimental conditions investigated ($4\,K < T < 500\,K$; $0.1\,atm < P < 20\,atm$). The response of S, R to 1 atm hydrogen at 500 K is consistent with the introduction of a new scattering channel for electrons/holes in the metallic tubes. Raman scattering from the Q-branch of hydrogen molecules adsorbed on the surface is found shifted only by 1–2 cm^{-1} from their frequencies in the free molecule and indicates that two different adsorption sites can be detected. Finally, H_2 wt% storage in heavily processed ropes of SWNTs are found to exceed 6% at $\sim$1 atm and $T = 77$ K and the isosteric heat of adsorption is found to be 120 meV.

PACS: 73.50.Lw; 61.46.+w; 72.80.Rj

Keywords: SWNTs; Thermoelectric power; Hydrogen storage

Ropes or bundles of single-walled carbon nanotubes (SWNT) provide an excellent opportunity to study the interaction of molecules and atoms with a simple physical surface. This stems from the geometry of the rope which is a close-packed bundle of several hundred, very long "pipes" whose mean diameter and wall thickness are $\sim$14 and $\sim$1.5 Å, respectively. For small molecules or atoms, e.g., N_2, H_2, O_2, He, Ar, etc., the internal diameter of the pipe is sufficient to allow gas storage within the pipe. The bundle structure of SWNTs produces at least four distinct sites in which gas molecules can adsorb (see Fig. 1): on the external bundle surface, in a groove formed at the contact between adjacent tubes on the outside of the bundle, within an interior pore of an individual tube, and inside an interstitial channel formed at the contact of three tubes in the bundle interior. For a particular gas molecule, some of these sites can be excluded on size considerations alone (assuming the bundle or tube does not swell to accommodate the adsorbed molecule). For example, the interstitial channel is approximately equal to the kinetic diameter of the

*Corresponding author. Tel.: 814-865-5233; fax: 814-865-9851.

E-mail address: pce3@psu.edu (P.C. Eklund).

[1] Present address: Technische Universiteit, Department of Applied Physics, Lorentzweg 1, 2628 CJ Delft, the Netherlands.

0921-4526/02/$ - see front matter
PII: S0921-4526(02)00994-8

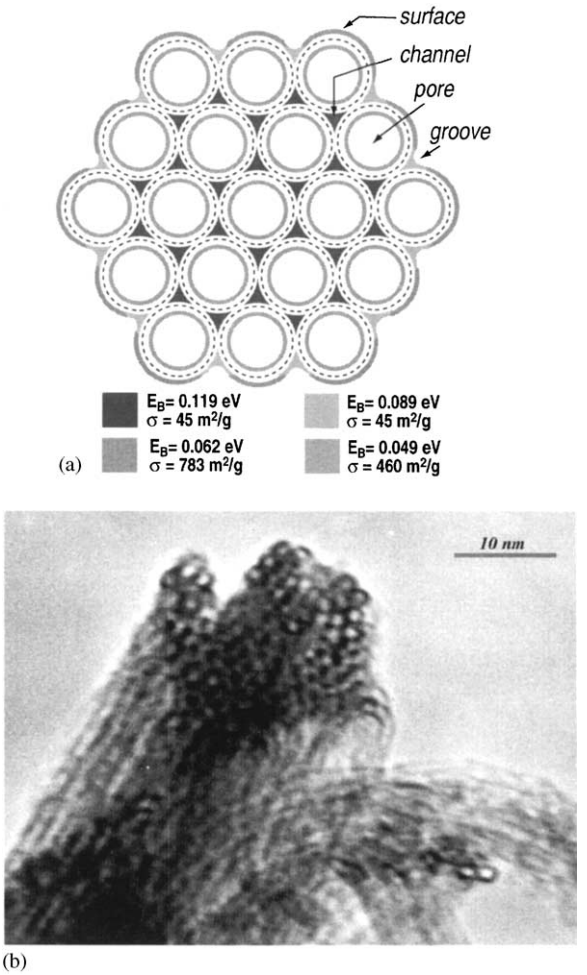

Fig. 1. (a) Schematic structure of a single-wall carbon nanotube bundle showing the pore, groove, channel and surface sites available for gas adsorption. Dashed line indicates the nuclear skeleton of the nanotubes. Binding energies (E_B) and SSA contributions (σ) for hydrogen adsorption on these sites are indicated. (b) High-resolution TEM image of end view of the SWNT bundles synthesized by arc-discharge method.

H_2 molecule. For hydrogen, calculations ignoring swelling have ordered the binding energy (E_B) in these various sites (c.f. Fig. 1(a)) as E_B (channels) > E_B(grooves) > E_B(pores) > E_B(surface) [1,2]. Access of molecules to the internal tube pores must either be through open SWNT ends or through defects (holes) in the tube walls. It is commonly believed that these gateways must be produced by post-synthesis chemical treatment. In this paper, we present results of thermoelectric transport, gas adsorption, and Raman scattering, which probe the details of the gas–SWNT interaction. We emphasize experimental results involving the interaction and storage of hydrogen.

Our studies were made on mats of tangled SWNT bundles. This arc-derived material was obtained from Carbolex, Inc., and consists of $\sim$50–70 vol% carbon as SWNTs. Transmission electron microscopy (TEM) showed that the material consists of several microns long bundles of SWNTs with mean bundle diameter $\sim$15 nm. Raman spectra, using a variety of excitation wavelengths, were found similar to those reported earlier for arc-derived material [3,4], exhibiting resonantly enhanced scattering from tangential ($\sim$1592 cm^{-1}) and several radial bands $160 < \omega_r < 200\,\mathrm{cm}^{-1}$. The radial-mode frequencies observed for these electric-arc-derived tubes indicate that the mean tube diameter is close to $\sim$1.4 nm. Two type-K thermocouples and two additional Cu wires for current leads made both thermal and electrical contact to the mat via silver-loaded epoxy. The four-probe AC resistance ($\sim$100 Hz) and the thermoelectric power were measured in situ in an apparatus which can be used to vacuum degas the mat or study the electrical response to high-purity (99.999%) gases in the temperature range $4\,\mathrm{K} < T < 500\,\mathrm{K}$.

In Fig. 2a and b we display, respectively, the normalized four-probe resistance (R/R_A) and thermopower (S) of a mat of as-prepared carbon nanotubes vs. time during vacuum degassing and subsequent exposure to N_2 and He gas at 1 atm. The experiments were conducted at 500 K. Open and closed symbols, respectively, refer to periods of vacuum (10^{-6} Torr) and gas exposure ($\sim$1 atm). In Fig. 2a, R/R_A is seen to decrease strongly during the initial degas, and then to rebound when the sample is exposed to N_2 or He. Note that the response times to these treatments are long (several hours), indicating that the diffusion of the gas in and out of the SWNT ropes is the rate-limiting process. In the case of the thermopower S (Fig. 2b), vacuum degassing at 500 K changes the sign of the thermopower. As pointed out previously [5], O_2-doped SWNTs are considered to be p-type because the chemisorbed O_2 acts as an

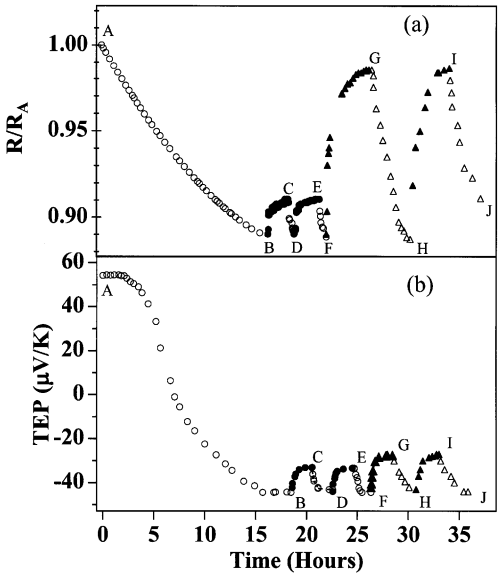

Fig. 2. (a) Four-probe resistance ratio vs. time for a mat of SWNTs at $T = 500$ K initially saturated with air at ambient conditions. Data normalized to sample resistance at A. The sample is under dynamic vacuum when open symbols are used, and dark symbols represent intervals where N_2 and He are present. N_2 is introduced at B and D; He is introduced at F and H. Vacuum pumping is applied at A, C, E, G, and I. (b) Thermopower S at 500 K vs. time. Sample was initially air saturated. Points A–I have the same meaning as described in the caption to Fig. 2a.

acceptor. Theoretical calculations indicate that O_2 is present as $O_2^{-\delta}$, $\delta = 0.1e$ [6]. The reason for the negative thermopower of the degassed mat is not well understood. We have pointed out that $S<0$ could be derived from low-lying wall defect states which act as donors, but this proposal needs further experimental proof [7]. We have included Fig. 2 to indicate that the thermopower and resistance of the mat are sensitive to gas exposure. This observation, at first, seems surprising for "inert" or non-reactive gases such as He, N_2. We have observed various responses ΔS and ΔR for isothermal exposure of degassed mats to many gases (e.g., NH_3, H_2, benzene, pyridine, etc. [8]). In general, $\Delta R/R_0 > 0$, unless charge transfer between the particular gas and SWNT is suspected, e.g., $NH_3^{+\delta}$ [9]. We have proposed [5] that ΔR is usually >0 because a new carrier scattering mechanism in the SWNT wall is created due to adsorbed gas, or to collisions of the gas molecules with the wall creating localized phonons. Furthermore, it is clear that ΔR can be <0 when charge transfer increases the carrier concentration (e.g., O_2, NH_3, C_5NH_5 (pyridine) [8]). The thermoelectric response can be positive or negative. This is more difficult to understand and may be associated with the free carrier details of the scattering process, as we discuss below.

In Fig. 3, we display the time response of the thermopower of vacuum-degassed mats to hydrogen at 500 K. Data are shown for three samples: as-prepared sample with 6 atomic (at.) % Ni, and two samples: which received the same selective oxidation step (425 C; 20 min) followed by, in one case a 4 h reflux in HCl (2 at.% Ni), and in the other case a 28 h reflux in HCl (0.2 at.% Ni). The metal content in each case was determined by ash analysis (combustion in dry air) in a gravimetric apparatus. As we have mentioned above, the *initial* degassed thermopower S_0 (time $t = 0$) depends on the sample history (e.g., as prepared, or acid reflux, etc.). *However, the change in the thermopower upon exposure to H_2 (ΔS) is relatively*

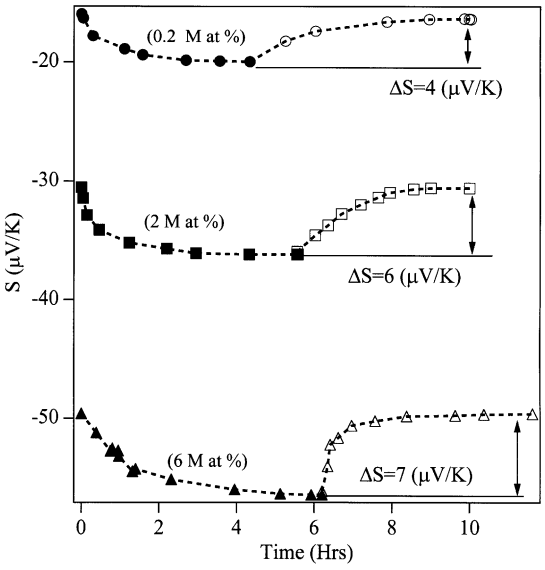

Fig. 3. In situ thermopower (S) vs. time (t) after exposure of degassed SWNT mats to a 1 atm overpressure of H_2 at 500 K (solid symbols). Open symbols are the response of the H_2 loaded SWNT system to a vacuum. Data are shown for three samples: (bottom) not purified, (middle) HCl reflux for 4 h, (top) HCl reflux for 28 h.

sample independent [10], *as can be seen from Fig. 3*. From Figs. 2 and 3, it may be noted that H_2 induces the opposite sign ΔS as observed for N_2 and He. This is also discussed below.

Our model for the thermopower of the mat is as follows. Details will be presented in a future publication [7]. The thermopower of the mat is not affected by the contact resistance between ropes, as S is related to the open-circuit voltage. The thermopower for a rope is the sum of conductivity-weighted contributions from the parallel semiconducting and metallic tubes. S is therefore dominated by the metallic tubes. The simplest behavior for a metal is $S \sim T$ at high T. The chemical potential (Fermi energy) for the rope is set by the balance of acceptor and donor impurities. Depending on the detailed balance of these impurity types, S is either positive or negative, and should exhibit an approximately linear T-dependence.

In Fig. 4, we show the T-dependence of S for a sample "purified" first by selective oxidation at 425°C in dry air for $\sim$20 min (to remove amorphous carbon) followed by an acid reflux in 4.0 M HCl to remove metal. A series of curves $S(T)$ are observed for the same sample after successively longer periods of vacuum degassing which removes successively larger amounts of O_2 from the ropes. We note from the figure that it is possible to generate a sample with $S \sim 0$ over almost the entire range of temperature from 4 to 300 K. We identify this behavior with a "compensated" sample, where the effects of donor and acceptor states cancel out. As mentioned above, we tentatively assign the donor states to wall defects.

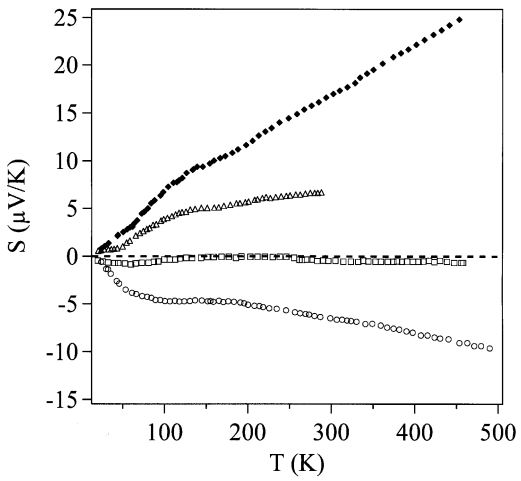

Fig. 4. Temperature dependence of thermopower S for a purified sample after successively longer periods of vacuum degassing which removes successively larger amounts of O_2 from the ropes.

Here, we wish to concentrate on the hydrogen:SWNT interaction. The previous discussion shows that the thermoelectric response of SWNT mats to hydrogen is very different from that observed for exposure to N_2 and He, for example. To provide a possible explanation for this observation, we write down an expression for ΔS, the thermoelectric response of the mat to gas exposure, due to an additional scattering channel introduced by the gas:SWNT interaction. The expression follows from the Mott relation [11] between the resistivity $\rho(E)$ and the thermopower S given by

$$S = (\pi^2 k_B^2/3e)T\{\mathrm{d}/\mathrm{d}E \ln \rho(E)\}_{E_F}, \quad (1)$$

where e is the magnitude of the charge on the electron, k_B is Boltzmann's constant, E_F is the Fermi energy, and T is the temperature. According to Matheissen's rule, the resistivity is the sum of contributions from separate mechanisms:

$$\rho = \rho_0 + \rho_I, \quad (2)$$

where ρ_0 is the resistivity of the degassed mat and ρ_I is the additional contribution due to impurity scattering associated with the gas:SWNT interaction. To arrive at the desired expression, we also need the well-known relation:

$$\sigma(E) = (\rho(E))^{-1} = e^2 v(E)^2 D(E)\tau(E), \quad (3)$$

where, v, D and τ are, respectively, the free carrier velocity, density of states, and carrier lifetime. It is then easy to show that in the limit $\rho_0 \gg \rho_I$

$$S = S_0 + (\pi^2 k_B^2 T/3e)(\rho_I/\rho_0)[(1/\tau_I)(\mathrm{d}\tau_I/\mathrm{d}E) - (1/\tau_0)(\mathrm{d}\tau_0/\mathrm{d}E)] \quad (4)$$

or

$$S = S_0 + \Delta S(\rho_I).$$

We see that the thermoelectric response of the SWNT to the gas depends linearly on the resistive

response $\Delta R \sim \rho_I$. From Eq. (4), we also note that the sign of ΔS can be >0 or <0, depending on the term in the brackets. It is important to note that Eq. (4) is derived for the case where E_F is a constant, i.e., physisorption *not* chemisorption is taking place.

In Fig. 5, we plot the thermoelectric power $S = S_0 + \Delta S$ vs. ΔR. From Eq. (4) above, we expect a linear relationship *if* the chemical potential (Fermi energy) is constant and the gas–SWNT interaction simply introduces a new impurity-scattering channel. As can be seen, all the data exhibit linear behavior consistent with our model assumptions. A non-linear relationship of S vs. ΔR would be expected if significant charge transfer occurs between the gas and the SWNT, as we have observed for O_2 [5] and NH_3 [9], where weak charge transfer is expected. It is interesting that $\Delta S/\Delta R$ has opposite signs for N_2 and H_2 exposure (Fig. 5). This can be understood if $(1/\tau_I)$ $(d\tau_I/dE)$ is gas dependent, consistent with a significant difference in the adsorption potential and/or adsorption sites for these two gases. Calculations to investigate this contention are now underway [7].

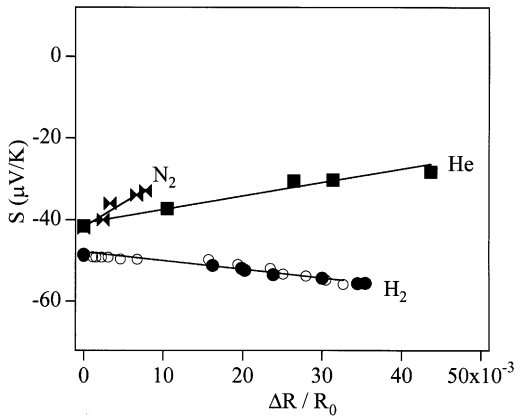

Fig. 5. Nordheim–Gorter ($N-G$) plots (S vs. $\Delta R/R_0$) for N_2, He, and H_2 showing the effect of gas adsorption on the electrical properties of the mat. A linear $N-G$ plot indicates that physisorption is taking place.

In Fig. 6, we display the Raman scattering spectrum from molecular hydrogen in contact with SWNTs, crystalline C_{60}, and highly oriented pyrolytic graphite HOPG [12]. The experiments were carried out at $T = 85$ K with the sample in an optical cell filled with an overpressure of 4–8 atm of H_2. The data are represented by the dots, and the solid line represents the fit to the data resulting from the sum of several individual bands (dashed lines). As a result of the H_2 gas in the optical cell,

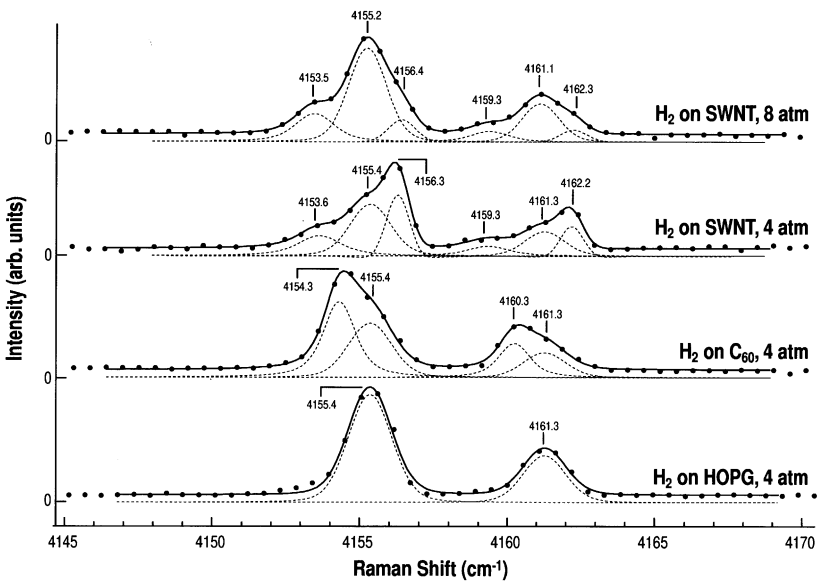

Fig. 6. Q-branch data for H_2 on SWNT at 8 and 4 ~ atm, together with data for C_{60} and HOPG at 4 ~ atm.

we observe bands at ~ 4161 and $\sim 4155\,cm^{-1}$. These should be the only bands visible in the case of experiments using the slab of HOPG, as H_2 should not intercalate between the graphene layers (bottom spectrum, Fig. 6). As can be seen in the figure, these "gas" lines in the HOPG spectrum are also resolved in the spectrum collected when the laser is focused on the surface of C_{60} and SWNT.

In addition, other bands are also observed for C_{60} and SWNT, which we identify with H_2 residing in these materials. In the case of C_{60}, the additional bands are downshifted by $\sim 1\,cm^{-1}$ relative to the gas lines. These are identified with H_2 which has diffused into the octahedral voids in the C_{60} lattice, consistent with neutron diffraction results [13]. The top two spectra in Fig. 5 are for H_2 in contact with SWNT bundles at 4 and 8 atm H_2 overpressure, respectively. The gas lines at $\sim 4161, 4155\,cm^{-1}$ nearly double in intensity as the pressure is doubled, as expected. In addition, we observe two new bands for each H_2 gas line: one upshifted by $\sim 1\,cm^{-1}$, the other downshifted by $\sim 2\,cm^{-1}$. These new bands are identified with H_2 physisorbed at two different sites in the rope. Contrary to reports on certain zeolites and oxides, which present ionic channels to the adsorbates, no strongly shifted Q-branch lines are observed in our experiments. This observation would seem to rule out significant charge transfer between H_2 and the SWNT, at least under the conditions of exposure here ($T < 300\,K$, $P < 8\,atm$). Theoretical calculations [12] of the anticipated shifts in the Q-branch modes for H_2 physisorbed on graphene are also found to be small, and in reasonable agreement with our experimental data.

In Fig. 7, we show low-temperature isotherms of the H_2 mass uptake for samples A (as prepared SWNTs), B (selective oxidation followed by HCl reflux for 4 h, then vac. annealed for 20 h at 1000°C) and C (selective oxidation followed by HNO_3 reflux for 24 h and vac. annealed for 20 h at 1000°C). HCl is a mild acid that does not appear to seriously attack the tube walls. HNO_3 reflux, however, is observed by HRTEM to cause serious damage that can be largely, but not completely, reversed by the high-temperature vacuum anneal. Hydrogen storage was studied on 75 mg samples. Data were collected gravimetrically and corrected

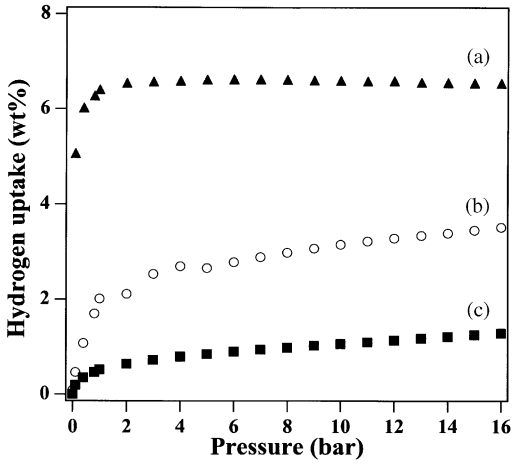

Fig. 7. Hydrogen isotherms ($T = 77\,K$) showing progressively better wt% H_2 storage with nanotube processing. From bottom to top: (a) the isotherms were taken on as-received material, (b) after selective oxidation/mild HCl reflux, followed by a heat treatment at 1000°C in vacuum (10^{-7} Torr) for 20 h, and (c) after selective oxidation followed by aggressive HNO_3 reflux, followed by a heat treatment at 1000°C in vacuum (10^{-7} Torr) for 20 h.

for buoyancy using a high-pressure thermo-gravimetric analyzer (TGA) (model # IGA-3, Hiden, Inc.). Ultra high purity (UHP) H_2 (99.999%) passed through an oxygen/moisture trap (Mega-Sorb Gas Purifier, Supelco, Inc.) and was introduced into the TGA. It should be noted that specific surface area (SSA) was measured in situ in the TGA just prior to H_2 loading. The SSA values for A, B and C samples are 270, 470 and 250 m^2/g, respectively. They are very low compared to the geometric surface area. Furthermore, we find that the SSA does not correlate with wt% H_2 storage, suggesting that the N_2 molecules are too large to probe the sites responsible for the H_2 adsorption. Although the geometrical surface area associated with the internal pore surface of a ~ 1.4 nm diameter SWNT is $\sim 1350\,m^2/g$, no one to our knowledge has reported values exceeding $\sim 400\,m^2/g$ for SWNT materials.[2] This indicates that the N_2 molecule is too large to gain access to many of these internal pores in a "real" material, despite the fact that the mean internal pore

[2] Recent studies on HiPCo purified SWNTs showed SSA as large as $1000\,m^3/g$.

diameter is ~ 1 nm. As pointed out previously [14], this may be associated with carboxylic acid and other functional groups that are attached to C-atoms present around holes in the tube walls, or at open tube ends. Apparently, most of the real gateways to the internal pore of the SWNT are apparently big enough to block N_2, but not H_2. The wt% H_2 stored in Fig. 7 is referenced to the real weight of the sample; no correction has been made for residual metal, etc. We compared $T = 77$ K isotherms for hydrogen and deuterium (D_2) on one of the purified samples; data were first collected with H_2. Next, the same sample was degassed in vacuum to 200°C for 12 h and then cooled to 77 K to collect the D_2 isotherm. The wt% storage found for D_2 not only confirmed the high storage observed for H_2 at low pressure in the same sample, but also revealed the effect of the quantum mechanical zero-point motion on the storage. That is, we observed wt% (D_2) > 2 times the wt% (H_2), i.e., the D_2 storage is larger than a simple "factor-of-two" enhancement stemming from the larger isotopic mass of D_2. At $T = 77$ K, we observed $\{\text{wt\%}(D_2)/\text{wt\%}(H_2)\} = 2.4$. It is known that the enhancement in the surface binding energy of deuterium over hydrogen is approximately proportional to $\frac{1}{2}$ the mean kinetic energy of vibration ($\langle \text{KE} \rangle$) of the molecule in the pore [15]. $\langle \text{KE} \rangle$ depends on the nature of the confinement of the molecule in the pore (e.g., interstitial channels in the bundle, internal pore of an individual nanotube), and thus the size of the isotope effect can give indirect information on pore volume and shape [15].

The isosteric heat of adsorption ($q_{\text{st}} = R\text{d}(\ln P)/\text{d}(1/T)$, where R is the gas constant) is a measure of the binding energy of the molecule to the surface. We can estimate this quantity using data from isotherms collected at two relatively close temperatures [16]. Using the $T = 77$ and 87 K isotherms for our best storage sample (C), we find that isosteric heat is 120 ± 5 meV. The isosteric heat bears a simple relation to the binding energy only within certain models or regimes of behavior. For example, a low-density gas on a planar surface obeys $q_{\text{st}} = \langle E_z \rangle + (3/2)kT$, where $\langle E_z \rangle$ is the mean binding energy of surface-normal motion, computed quantum mechanically. At $T = 77$ K, it should be noted that $kT \sim 6$ meV. So in our case, we expect that the isosteric heat and the binding energy are nearly equal, independent of the details of the confinement.

The most remarkable feature of all the data in Fig. 7 is the very low H_2 overpressure required for significant storage in the processed SWNT material. We can compare our data for the HNO_3-treated material to that of Ye et al. [17] who reported a maximum of ~ 8 wt% storage at $T =$ 77 and ~ 100 atm. Their pressures are a factor of 20–40 higher than required in our material to achieve the same storage. This remarkable change in the pressure scale suggests to us that the disorder we have created in the SWNT walls and bundling as a result of aggressive HNO_3 reflux may play an important role in enhancing the binding energy for H_2 adsorption.

This work was supported by ONR, NSF (PSU MRSEC), Honda Motors. Many valuable discussions with Profs. Gerald Mahan, Milton Cole, and Vincent Crespi are gratefully acknowledged.

References

[1] K.A. Williams, P.C. Eklund, Chem. Phys. Lett. 320 (2000) 352.
[2] G. Stan, M.W. Cole, J. Low Temp. Phys. 110 (1998) 539.
[3] M.S. Dresselhaus, P.C. Eklund, Adv. Phys. 49 (2000) 705.
[4] A.M. Rao, et al., Science 275 (1997) 187.
[5] G.U. Sumanasekera, C.A.K. Adu, S. Fang, P.C. Eklund, Phys. Rev. Lett. 85 (2000) 1096.
[6] S.H. Jhi, S.G. Louie, M.L. Cohen, Phys. Rev. Lett. 85 (2000) 1710.
[7] H.E. Romero, et al., Phys. Rev. B 65 (2002).
[8] G.U. Sumanaskera, et al., Phys. Rev. Lett., (submitted).
[9] C.K.W. Adu, et al., Chem. Phys. Lett. 337 (2001) 31.
[10] G.U. Sumanasekera, et al., Phys. Rev. B 65 (2002) 035408.
[11] R.D. Barnard, Thermoelectricity in Metal and Alloys, Wiley, New York, 1972.
[12] K.A. Williams, et al., Phys. Rev. Lett. 88 (2002) 165502.
[13] S.A. Fitzgerald, et al., Phys. Rev. B 60 (1999) 6439.
[14] D.B. Mawhinney, et al., Chem. Phys. Lett. 324 (2000) 213.
[15] M.K. Kostov, et al., Chem. Phys. Lett. 332 (2002) 26.
[16] S.J. Gregg, K.S.W. Sing, Adsorption, Surface Area and Porosity, Academic Press, London, 1982.
[17] Y. Ye, et al., Appl. Phys. Lett. 74 (1999) 2307.